Available online at www.eccomasproceedia.org
Eccomas Proceedia COMPDYN (2021) 3589-3604

ECCOMAS
Proceedia

COMPDYN 2021
8th ECCOMAS Thematic Conference on
Computational Methods in Structural Dynamics and Earthquake Engineering
M. Papadrakakis, M. Fragiadakis (eds.)
Streamed from Athens, Greece, 28 - 30 June 2021

ON THE SITE-AMPLIFICATION AND SOIL-STRUCTURE INTERACTION IN URM STRUCTURES: USE OF FRAGILITY CURVES TO ASSESS THE SIMPLIFIED CODE-APPROACH

A. Brunelli[1], F. de Silva[2], and S. Cattari[1]

[1] University of Genoa
Genoa, Italy
andrea.brunelli@edu.unige.it, serena.cattari@unige.it

[2] University of Naples Federico II
Naples, Italy
filomena.desilva@unina.it

Abstract

The paper investigates the effects of site-amplification and soil-foundation-structure interaction (SFS) on the fragility curves of a real unreinforced masonry (URM) structure. The building is inspired to a school with an irregular T-shape plan and is modelled according to the equivalent frame approach. The structure was ideally placed on a stiff rock outcrop (case FB A) or settled on four different soft soil profiles, including its real foundation subsoil. In the latter cases the base of the structural model was assumed as fixed (FB C) or endowed with springs (CB C) simulating the soil-foundation dynamic impedance. To evaluate the fragility curves, the corresponding structural models were analysed through non-linear dynamic analyses under 136 input motions, propagated in 1D soil models reproducing the selected profiles for FB C and CB C. The results were compared in the paper in terms of:
-fragility curves calculated for five damage levels (defined to be conceptually consistent with those of the EMS98 scale) and expressed as a function of different intensity measures of the input motion;
- average damage derived as a weighted average of the probability of failure associated to all the damage levels.
The comparison among the results of the different models highlights the expected increase of damage due to site effects and a beneficial effect of soil-structure interaction, mainly due to the increment of damping associated to the additional energy dissipated by the soil-foundation system. Finally, the average damage of FB C and CB C models were compared with those obtained from the fragility curves of a fixed base system in which site effects are considered through the conventional coefficients proposed in Codes (e.g. by the Eurocode 8), that neglect SFS. This latter approach is that followed in the current practice. The comparison demonstrates that the Code-based approach underestimates the fragility especially at high damage levels.

Keywords: seismic site amplification, soil-structure interaction, fragility curves, unreinforced masonry structures, nonlinear dynamic analyses, code prevision.

ISSN:2623-3347 © 2021 The Authors. Published by Eccomas Proceedia.
Peer-review under responsibility of the organizing committee of COMPDYN 2021.
doi: 10.7712/120121.8732.18903

1 INTRODUCTION

Various reconnaissance studies after seismic events [1, 2, 3] as well as more specific studies at scale of whole historical centres [4, 5, 6] testified as the site-amplification effects (either associated to topographic and soil stratigraphic effects) may play a relevant role, together with their vulnerability, in determining the resulting damage levels on existing unreinforced (URM) masonry. The microzonation studies, developed in various area in Italy after the recent seismic events [7, 8] that hit the country, confirmed this potential risk factor.

Together with this evidence at large scale or on huge building stocks, studies based on detailed models of prototype buildings and more refined analyses methods turn out very useful to understand the phenomenon and also deepen the potential effect of the soil-foundation-structure interaction (SFS). In [9] the topic is treated in a parametric way to attempt in providing a general overview of such effects on various structural typologies (classifiable according to their dynamic behaviour as "stiff" or "flexible") concluding how the SFS may produce either beneficial or detrimental effects. The literature works specifically addressed to URM buildings are still very few, and usually focused to slender structures, like as towers or minarets [10, 11, 12], or massive monumental assets, like as fortresses [13, 14]. A recent very interesting case, that testified the possible role of SFS also on ordinary URM buildings, is constituted by the "P. Capuzi" school in Visso (MC, Italy). Being monitored as a strategic building by the Italian Seismic Observatory of Structures [15], the school response under the three mainshocks of the 2016-2017 Central Italy earthquake was recorded through numerous accelerometers installed in the building as well as the damage after each event was detected through on-site inspections. Although nowadays the school has been demolished due to the very severe damage occurred, all the precious data collected were very useful to validate numerical models and assess the role played by SFS phenomena in the seismic response of the school, like by [16, 17].

In particular, in [16] a compliant-base model has been successfully validated thanks to these data. This model, that works according to the equivalent frame modelling approach, is the one adopted also for the further developments presented in this paper, which focuses to both the site-amplification due to soil stratigraphic effects and the role played by SFS.

More specifically, the numerical strategy validated in [16] thanks to the actual recordings from the 2016-2017 Central Italy earthquake has been replicated by executing a huge set of nonlinear dynamic analyses (NLDA) with the final aim of developing fragility curves, similarly to what done for example by [5, 18, 19]. The model (briefly recalled at §2.3) has been analysed both as fixed at the base (FB) and endowed with springs (CB) simulating the soil-foundation dynamic impedance. NLDA have been performed according to the Cloud Method (see e.g. [20]) with a selection of records extracted from the SIMBAD database in [21, 22] to be representative of real events recorded on stiff rock outcrop. Then, they have been propagated by considering four different soft soil profiles (§2.1) representative of a class soil C (according to classification adopted in [23, 24]), including the real foundation subsoil of the school (§2.2). Fragility curves are defined assuming a log-normal distribution. The structural response from NLDA is interpreted according to a multiscale approach briefly described at §2, that allows to attribute to each records a damage level, defined to be conceptually consistent with those of the EMS98 scale [25]. Moreover, different intensity measures of the input motion have been considered in order to assess the sensitivity to the dispersion in the definition of the fragility curves (§3.1), namely the Peak Ground Acceleration (PGA) and the Spectral Acceleration corresponding to the fundamental period of the structure ($Sa(T_1)$).

Finally, the average damage of FB C and CB C models were compared with those obtained from the fragility curves of a fixed base system in which site effects are considered in a simplified way through the conventional coefficients proposed in Codes (e.g. by the Eurocode 8 [24]),

that neglect SFS (§3.2). This latter approach is that followed in the current practice. The comparison aims to assess if the current Code-based approach is on the safe side or not, also varying the expected damage level (i.e. the nonlinear phase attained by the structure).

2 METHOD OF ANALYSIS

As introduced at §1, in this study fragility curves of a URM building endowed with shallow foundations were calculated accounting for both the amplification of the ground motion due to site effects and the dynamic soil-foundation-structure (SFS) interaction. Due to the low foundation embedment, the foundation input motion is expected to be equal to the free field motion, hence the latter was calculated through linear-equivalent one-dimensional site response analyses performed on four soil profiles. The resulting ground motion (illustrated at §2.3) was then used as input motion to perform non-linear dynamic analyses on:
- a fixed base structural model (indicated as FB C in the following);
- a compliant base structural model in which the base of each main wall is equipped with springs (indicated as CB C in the following).

The rich and huge amount of data from each nonlinear dynamic analysis carried out are interpreted according to a multiscale approach with the final aim of interpreting the simulated structural response through a synthetic parameter consisting in the global damage level. The latter has been defined to be conceptually consistent with the five ones defined in the EMS98 scale [25], that is (DLi, i=0…5): DL0 - none; DL1 - negligible; DL2 - moderate; DL3 - severe; DL4 - very severe to near collapse; DL5 - collapse. In particular, the adopted multiscale approach, similarly to what originally proposed in [26], combines two heuristic criteria:

- a first one that directly refers to the global response scale, by defining proper thresholds of the displacement capacity of the building on pushover curves estimated from nonlinear static analyses. These thresholds are defined in terms of proper fractions of the overall base shear (V_b): before the attainment of the maximum value ($V_{b,max}$) to define the DL1 (equal to 0.4 $V_{b,max}$) and DL2 (equal to 0.8 $V_{b,max}$); after the attainment of the maximum value, i.e. on the softening phase of the curve, to define the DL3 (corresponding to a residual capacity equal to 0.8 $V_{b,max}$), DL4 (corresponding to a residual capacity equal to 0.4 $V_{b,max}$) and DL5 (corresponding to a residual capacity equal to 0.2 $V_{b,max}$).
- a second, based on the evaluation of damage severity and diffusion on vertical walls, that aims to monitor the spread of damage on the building. To this aim, the cumulative rate of walls that reached a given DL (graduated on five level) is computed. The attainment of the DL on a wall is checked in terms of the DL_{min} variable firstly introduced in [27]. This variable replaces the adoption of interstorey drift thresholds at the wall scale and the proposal assigns a damage level to the wall based on the minimum damage level attained by all the elements of a certain floor. This allows overcoming the definition of conventional interstory drift thresholds, which are not suited to take into account the different damage mechanism exhibited by structural elements of different slenderness. A similar damage-assignment criterion has been recently pursued in Italian Structural Code [28]. The thresholds assumed for the cumulative rate have been defined to be consistent with the linguistic description of the damage grades of buildings proposed by the European Macroseismic Scale [25]; they are described in more detail in [29, 30].

According to this procedure, results of records can be properly grouped as those associated to the same resulting global DL.
Then, fragility curves were computed by estimating the probability of exceeding, p_{DLi}, the different damage levels, DLi, given a level of ground shaking quantified through the intensity

measure, IM. The p_{DLi} was computed from the lognormal distribution of *IM* causing the i^{th} DL and characterized by the median value IM_{mi} and the lognormal standard deviation σ:

$$p_{DLi}(DL > DLi|IM) = \Phi\left(\frac{\log IM|IM_{mi}}{\sigma}\right) \quad (1)$$

Where Φ is the standard cumulative probability function.
Among possible intensity measures [31], in this study, the peak ground acceleration, PGA, and the spectral acceleration, $Sa(T_1)$ referred to the bedrock input motion were used as IM. This choice is consistent with various studies on URM buildings [32, 33, 34]. In particular, the geometrical mean of the PGA and the $Sa(T_1)$ associated to the predominant period along the X and Y directions of the numerical model was used. Since an elongation of the periods is expected for the compliant base models, the $Sa(T_1)$ of the CB C case differs from those of the FB C case, while the PGA is obviously the same for the two models.
On basis of this procedure, the fragility curves resulting from the FB C model account only for site effects, while those of the CB C model consider both the site and SFS effects. Both cases have been then compared with the fragility curves of the same structure ideally placed on a stiff rock outcrop. The latter were obtained by analyzing the behavior of the fixed-base model subjected to the input motions representative of the bedrock condition (namely the FB A case in the following).

2.1 Analysed soil profiles

To study the influence of the soil stiffness on the results of FB C and CB C cases, four soil profiles were selected. The criterion adopted for the selection is that based on an equivalent shear wave velocity up to the bedrock depth, V_{Seq}, falling in the range of class C (as defined by [23, 24]). The first profile (S1) is the actual soil below the "P. Capuzi" School of Visso, i.e. a sandy gravel layer (SG), covered and locally interbedded by clayey silt (CS) and silty clay (SC) lenses. The stiffness profile was measured through a MASW test [35] and several down-hole tests [36]. The on-site measured free field frequency obtained from HVSR tests allowed the back-calculation of the bedrock depth equal to 40 m. The shear wave velocity, V_S, is variable with depth with an equivalent value up to the bedrock equal to 281m/s. Additional details on the geotechnical characterization of this soil profiles are reported in [16].
The second profile (S2) is the actual soil in the historic centre of Visso, investigated through two boreholes and a HVSR test [36]. The profile is made of clayey silt (CS) for the first 4 m, overlaying a 11 m thick sandy gravel layer (SG). The geological section of the Visso valley reported by [36] individuates the bedrock at a depth of 18 m. In lack of a direct measure of V_S, its value was obtained through a correlations law between Vs and the number of blows of SPT tests performed at a depth of 1.9 m in CS and 4.4 and 8.9 m in SG, respectively. Before the application, numerous correlation law available in the literature were checked against the results of down hole tests in the same valley. Such validation is not reported here for sake of brevity. The most successful correlations in the validation were used to characterize S2. In particular, the correlations by [37, 38] were used for CS, leading to the same V_S=162 m/s, and by [39] for SG, leading to V_S=337 m/s. The consequent equivalent V_S up to the bedrock depth is V_{Seq}= 272 m/s. Finally, two other ideal clay (S3) and gravel (S4) profiles were considered with the bedrock placed at a depth of 40 m. In both cases Vs increases with depth. Its profile was calculated through the empirical laws by [40] for S3 and by [41] for S4, respectively. The resulting Vs_{eq} are 200 and 279 m/s, which are similar to those of S1 and S2.
Figure 1a summarizes the four soil and V_S profiles while Figure 1b reports their amplification functions. The latter have been calculated through a linear site response analysis performed by

using the STRATA software [42]. As highlighted by the resulting natural frequencies, there is a significant variety among the responses of the different soil profiles.

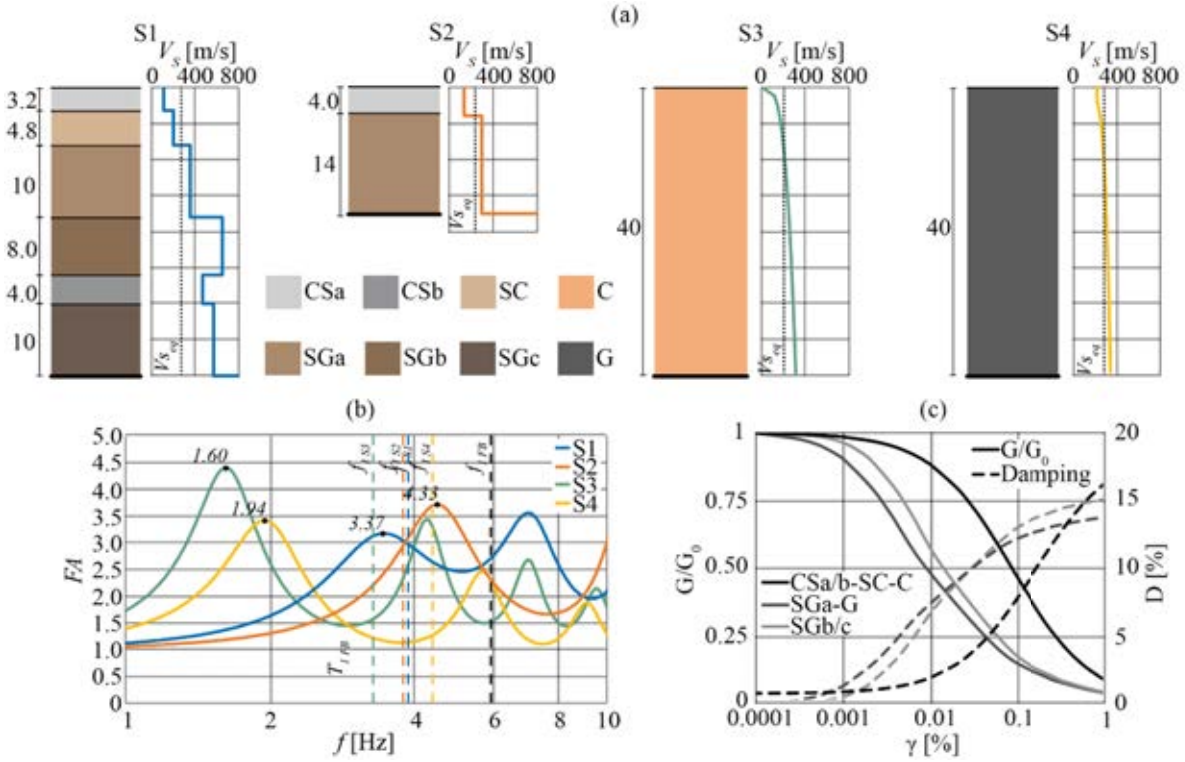

Figure 1: (a) layer with profile Vs; (b) FA of the four stratigraphies and (c) decay curves of the soils considered.

Finally, Figure 1c shows the variation of the normalized shear modulus (G/G_0) and the damping ratio (D) with the shear strain (γ) adopted in the linear equivalent site response analyses executed with the records of real earthquakes and performed again in the STRATA software. The curves adopted for the fine-grained soils in S1, S2 and S3 were obtained based on a comprehensive model calibrated by [43, 44] on the results of laboratory tests on comparable materials. The G/G_0-γ curves obtained by [45], through laboratory tests on silty sandy gravel samples different confining stress were associated to the sandy gravel soil in S1, S2 and S4. The corresponding D-γ curves were calculated by applying the model by [46] and the Masing criteria [47] to the G/G_0-γ curves.

2.2 Results of site response analyses under records of real earthquakes

Figure 2 shows the acceleration time histories of the input motions employed to analyse the site effects in the four soil profiles described in §2.1. They were chosen from the Selected Input Motions for Displacement-Based Assessment and Design (SIMBAD) database [21, 22].

The selection includes the EW (Channel 1 (C1)) and NS (Channel 2 (C2)) components of accelerations recorded during 49 natural events at stations located on stiff rock outcrop, *i.e.* Vs_{30} greater than 700 m/s. Some selected signals were slightly scaled to achieve the desired variability of the intensity measures to be used in the construction of the fragility curves of the FB A.

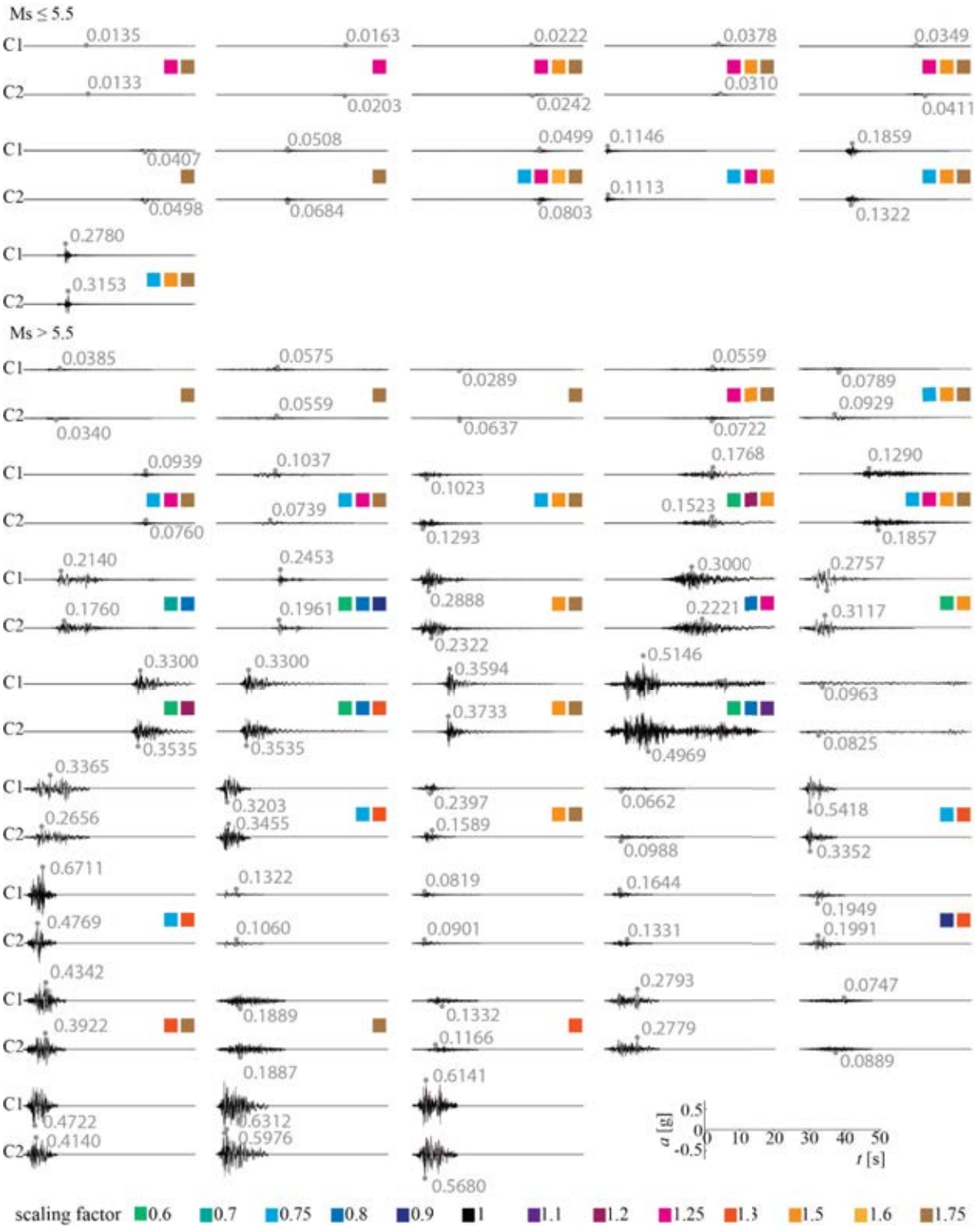

Figure 2: Time histories of the acceleration of the selected input motions.

Colours in Figure 2 indicate the scaling factors, when multiple colours are present, the same input motion was scaled more than once.

Figure 3 shows the mobilized G/G_0 (a) and hysteretic damping ratio (b) calculated in the four considered soil profiles through site response analyses under each event. The mean values

mobilized in the soil volume, expected to be affect by the foundation motion (i.e. 1 m under foundation level) are reported. As expected, the highest effects of nonlinearity are recognized: for the profile S3, characterized by the lowest initial stiffness; and the gravel soil profile S4, characterized by the earliest development of stiffness reduction (see Figure 1c). Conversely the lowest nonlinearity corresponds to the shallowest bedrock producing the highest natural frequency, *i.e.* the stiffest response (see Figure 1b). The actual soil profile below the school, S1, shows an intermediate behaviour.

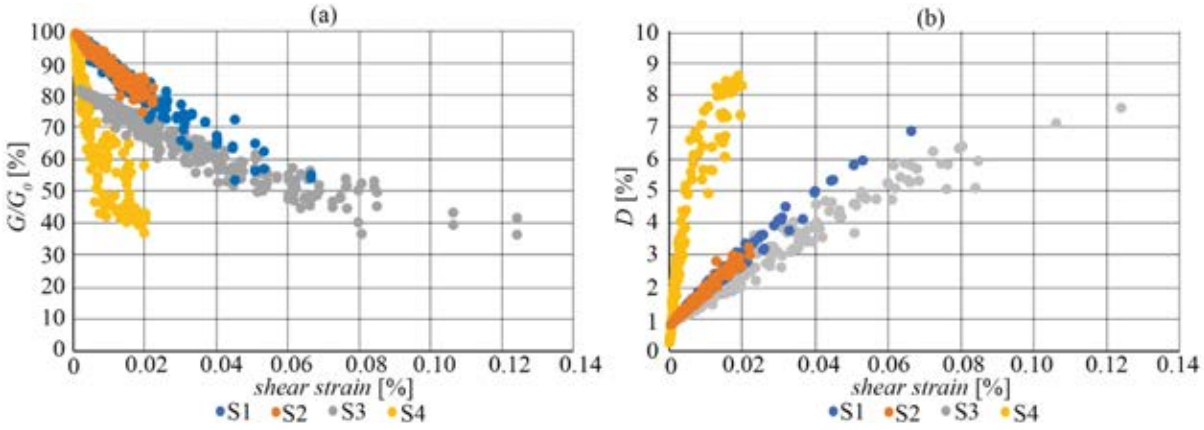

Figure 3: (a) G/G_0 and (b)hysteretic damping ratio mobilized in the four soil profiles in significant volume during each site response analysis.

Figure 4 groups the analyses according to different ranges of $Sa(T_1)$ of the free field motion resulting from the site response analyses and corresponding to the fixed-base period. The latter are reported in Table 1 together with the period of the CB models on the different soil profile, revealing that the different initial shear stiffness of the soil profiles significantly affects the CB C period.

Model	FB	CB -S1	CB -S2	CB -S3	CB -S4
T_1 [s]	0.1740	0.2580	0.2640	0.3050	0.2298

Table 1: first period of each model.

The comparison among the number of signals belonging to each group, reported in red on the top of Figure 4, shows that $Sa(T_1)$ values on surface of profile S4 are lower than 1.5 g and mainly concentrated in the lowest amplitude ranges. The ranges associated with the highest $Sa(T_1)$ are populated mainly by signals propagated in S1 and S3, highlighting that such profiles are more hazardous for the structural safety.
In the same Figure 4 the number of times in which $Sa(T_1)$ of the CB models exceeds that of the FB ones is reported in percentage on the Y-axis. Except for S2 showing a more irregular trend, such percentage increases with increasing $Sa(T_1)$ and is predominant (i.e. >50%) from $Sa(T_1)$>0.75 g. Hence, a detrimental effect of SFSI is shown on the seismic actions affecting the structure especially under the most severe input motions.

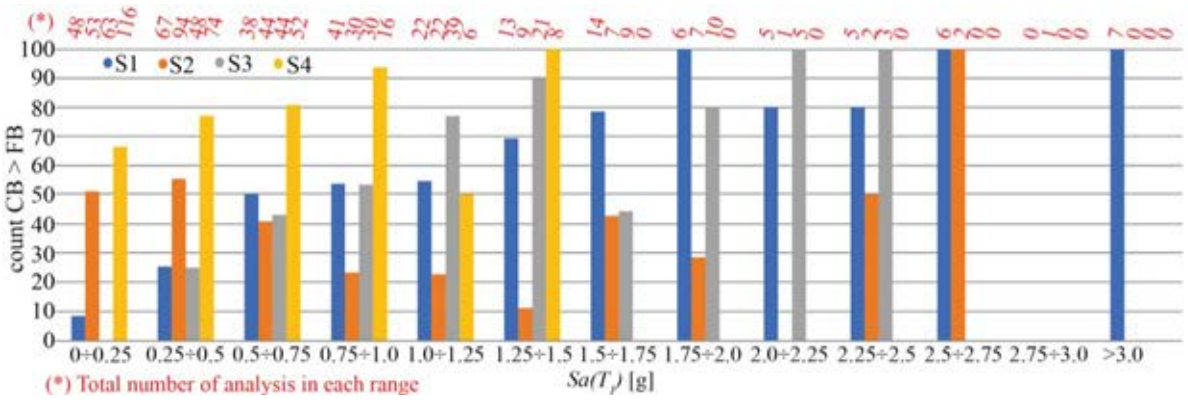

Figure 4: number of times in which Sa (T_1) of the CB model exceeds that of the FB.

2.3 Numerical model of the selected URM building

The 3D model of Visso school (Figure 5a) adopted for the execution of NLDA works according to the equivalent frame (EF) approach. It has been realized with the Tremuri software package [48] and has been calibrated in [16] thanks to the available data on the structure from the permanent monitoring and previous studies [35]. The choice of adopting the EF model is justified by the regular pattern of openings in walls and by the evidence from the actual seismic response [49], that clearly highlighted the concentration of cracks in specific portions of the walls (namely, the piers and spandrels, respectively identified in orange and green in Figure 5a).The constitutive law used allows for describing the nonlinear response until very severe damage levels at element scale (i.e. DL_E from 1 to 5) through progressive strength degradation corresponding to assigned drift values; with the aim of executing NLDA [34], the constitutive law includes also a hysteretic response (Figure 5b). The latter is based on a phenomenological approach that allows also to differentiate the hysteresis loops in spandrels and piers and also varying the prevailing failure mode (e.g. if dominated by the flexural response or diagonal shear cracking). For further details on mechanical panel properties and modelling assumptions the interested reader may refer to [16].

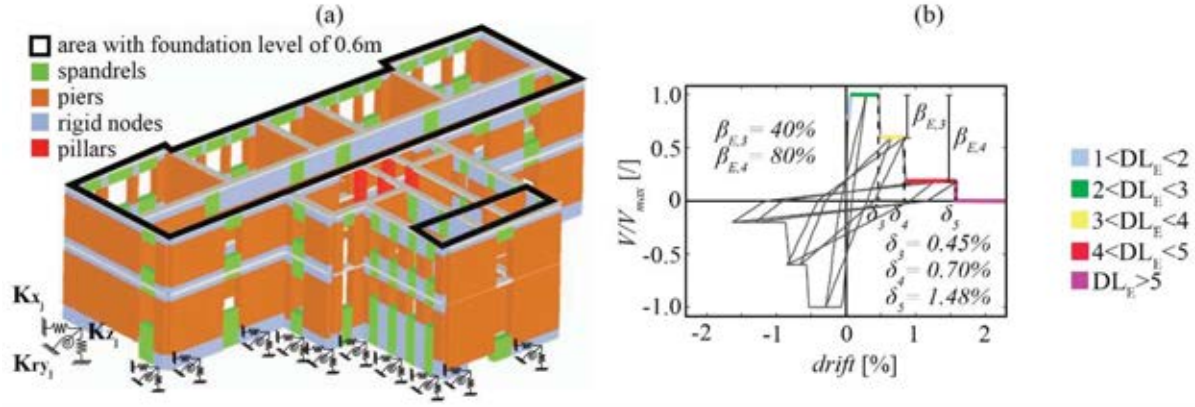

Figure 5: (a) 3D equivalent frame model with springs implemented in the CB model, (b) backbone and hysteretic response of masonry elements: piers under shear.

To simulate the base compliance, each foundation pier was equipped with springs (see Figure 5a), which stiffness was calibrated through the real part of the soil-foundation impedances by [50]. The foundation width was set equal to 0.90 m, while its length was defined by adding the

half-length of the spandrel panel to the size of the load-bearing wall. The value of the embedment was set to 0.6 m, except for the area indicated in Figure 5a, where the embedment increases up to 2.95 m due to the presence of an underground level. The soil was modelled as an equivalent linear half-space with a shear modulus equal to that mobilized at the foundation depth under each input motion. A full soil-foundation contact was assumed.
Firstly, the periods along the X and Y directions (T^*_x and T^*_y) and the damping ratio (β_x and β_y) of the SFS system were estimated through the replacement oscillator by [51]. To this aim, the building was approximated through a SDOF system with a viscous damping ratio equal to 3% and a lateral stiffness derived from the fundamental periods along the X and Y directions of the fixed base configuration (see [16]). To apply the formula by [51], the real and the imaginary parts of the monolithic foundation equivalent to the actual foundation systems were calculated from the sum of the real or imaginary parts of the impedances of the X-oriented (or Y-oriented) load-bearing walls. The contribution of the soil hysteretic damping mobilized at the foundation level (see Figure 3b) was added to the energy loss coefficients simulating the radiation damping ratio.
Then the frequency-dependent dynamic coefficients of the impedances were computed as a function of the resulting T^*_x and T^*_y, through an iterative procedure. To simulate the additional energy dissipation due to SFS interaction, the mean value of β_x and β_y was introduced as a Rayleigh damping ratio into the EF model. The calculation was repeated for each input motion: consequently, the impedances and the resulting T^*_x and T^*_y as well as the mean value of β_x and β_y, were updated according to the mobilized soil shear stiffness and damping ratio during each seismic response analysis (see Figure 3).

3 DESCRIPTION OF RESULTS

3.1 Influence of site effects and SSI on the fragility curves

Table 2 reports the number of analyses (N), the median value IM_{50} (in acceleration unit g) and the standard deviation (σ) used to generate the fragility curves of the fixed-base model analysed under the selected input motion (FB A).

Only few analyses, reported in brackets in Table 2, mobilize DL3, DL4 and DL5 for the FB A case; so the initial set of input motions described in Section 1.2 was integrated with the natural signals recorded on stiff soil and collected by [52]. However, the IM_{50} and σ resulting from the updated set of input motions are comparable with those obtained from the original selection (in brackets). There is only an increase, less than 10%, of the IM_{50} associated with DL5 in the case of PGA which results in a reduction of structural fragility.

	FB A				
	PGA		$Sa(T_1)$		
	IM_{50}	σ	IM_{50}	σ	N
DL1	0.095	0.495	0.178	0.473	127
DL2	0.274	0.314	0.656	0.391	92
DL3	0.450 (0.413)	0.219 (0.255)	1.013 (0.969)	0.376 (0.423)	18 (10)
DL4	0.530 (0.488)	0.191 (0.147)	1.182 (1.156)	0.308 (0.299)	17 (7)
DL5	0.619 (0.562)	0.219 (0.178)	1.500 (1.428)	0.261 (0.314)	44 (12)

Table 2: Median value (IM_{50}) and standard deviation (σ) associated with to the various damage levels for the FB A model.

It is worth to remember that the IMs calculated for FB C and CB C refer to the bedrock. This implies that the IM_{50} values reduce moving from the FB A to FB C, independently of the soil profile. That highlights the expected increase of fragility for a fixed-base structure settled on soil type C with respect to that placed on soil type A, as shown in Figure 6 by way of example in the case of DL3.

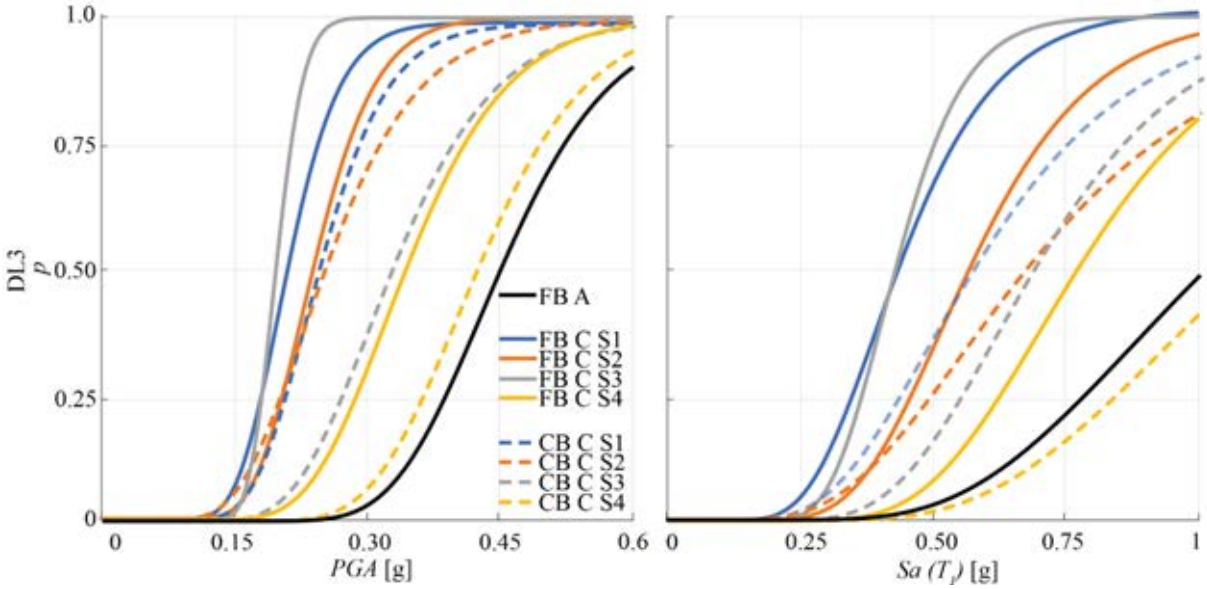

Figure 6: Comparisons between the curves obtained from the FB A, FB C and CB C assuming PGA and Sa (T_1) as IM in case of DL3.

The comparison with the CB C models reveals an increase of IM_{50} with respect to the FB C case. Such modification reduces the probability of failure on the building. Since the elongation of the CB C period produces an increment of the seismic actions with respect to the FB C case (see Figure 4 and Section 2.2), such beneficial effect is mainly due to the increase of damping ratio produced by the SFS interaction, as shown in Figure 6 by way of example for DL3. This general conclusion is however extendable to all DLs.

The same beneficial effect is evident by comparing the number of analyses that fall into the various DL_i for the FB C and CB C. There is in fact a reduction of the analyses in the more severe DLs for the CB C model, in particular for the profile S4 where the analyses in DL5 are only 3. Such reduced number of analyses reduces the reliability of the DL5 fragility curve for S4, hence this case will not be considered in the following interpretations. Obviously, the reliability of DL5 would have been improved by scaling through higher factors the signals originally selected, but such procedure would have led to unrealistically strong free field motions. Conversely, the low occurrence of DL5 for S4 (resulting from the numerical analyses) appeared much more realistic, because buildings settled on gravel are less prone to high damage since they are affected by lower seismic actions (see Figure 4) and benefit of higher soil damping.

The estimation of p_{DLi} through Equation 2 allows the computation of the mean damage μ_d expected to affect the structure, as follows:

$$\mu_d = \sum_{i=0}^{5} (p_{DLi}\, i) \tag{2}$$

where p_{DLi} is weighted by i=0,1,2,3,4 or 5 passing from DL0 to DL5.

The calculation was performed by entering the curves of the case FB C and CB C with the values of PGA and Sa(T_1), at the bedrock of each selected input motion. The μ_d value may be conveniently converted into an equivalent discrete damage level by assuming a binominal

distribution, leading to the following conversion intervals: 0-0.7 for DL0; 0.7-1.6 for DL1; 1.6-2.5 for DL2; 2.5-3.4 for DL3; 3.4-4.3 for DL4; 4.3-5 for DL5. The latter ones have been used to define the "square metric" in Figure 7. These comparisons are reported considering as IM: the PGA in (a); and the Sa(T_1) in (b). The grey fillings indicate a difference of 1, 2 or 3 DLs between the mean damage of FB C and CB C. In the case of the PGA, SFS interaction always leads to a reduction of the expected damage, independently of the soil profile and the greatest beneficial effects at DL3-4, specially for S3. Considering the Sa(T_1), the results are more dispersed. In any case there is a greater damage associated with the FB C model, but there are also some cases in which the CB C model leads to greater damage, specially at lowest DL in S1 and S2. In this case, it is worth to remind that also the IM changes among the models, because the fundamental period changes as shown in Table 1.

Despite these slight differences, the general conclusion on the SFS effects observed from the use of PGA and Sa(T_1) is the same.

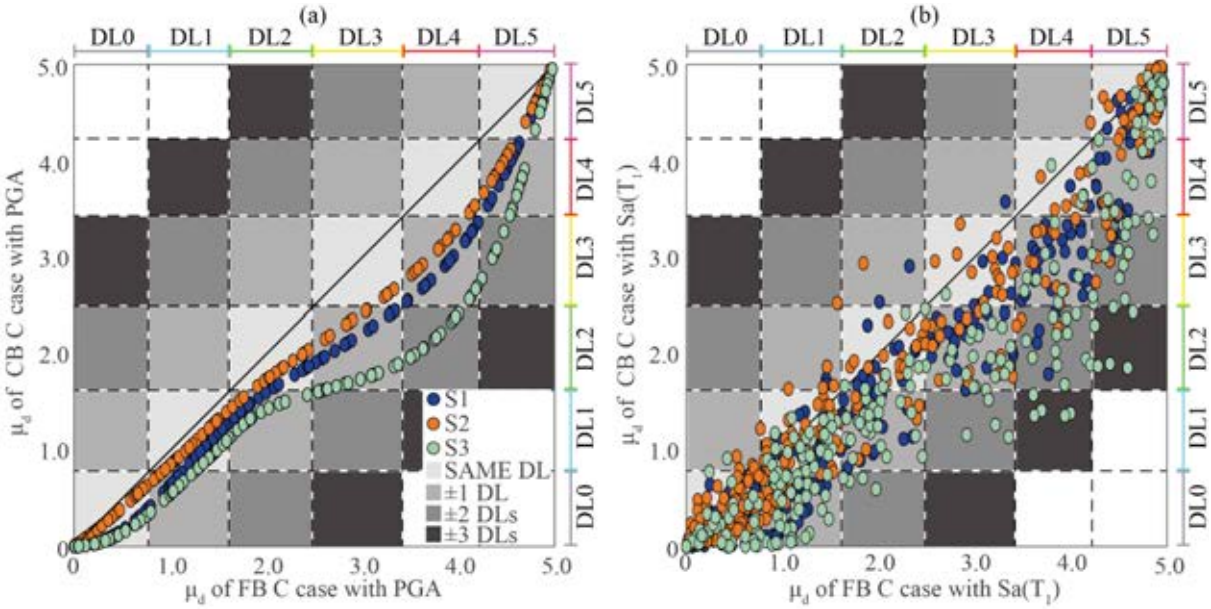

Figure 7: μ_d between FB C and CB C for S1, S2 and S3 in case of (a) PGA and (b) Sa(T_1).

3.2 Comparisons with the Eurocode previsions

In the most widespread cases of fragility curves generated for fixed base structures and stiff soil conditions (case FB A), site effects can be considered in the estimation of p_{DLi} in a simplified way, *i.e.* by entering in the curve with the IM amplified by the stratigraphic coefficient provided by Code. As an example, on the abscissa, Figure 8 shows the μ_d resulting from the fragility curve of FB A in which the terms p_{DLi} in Equation 2 alternatively corresponds to peak ground (PGA*) or the spectral (Sa(T_1)*) accelerations, amplified according to the coefficient proposed by the [24]. This is equal to 1.5 for events with a surface wave magnitude lower than 5.5; otherwise it is equal to 1.15 (see Figure 2). When only site effects are considered (FB C) (see Figure 8a and b), EC8 underestimates the damage in any case and up to three damage levels. Soil-structure interaction reduces the gap between the μ_d estimated through the Code conforming approaches and that estimated by explicitly accounting for the site effects joint to the soil structure interaction (CB C) (see Figure 8c and d). However, a difference of one DL (very rarely of two DLs) still results also for CB C. Such underestimation arguably would increase if the increment of damping ratio induced by SFS interaction was considered in the computation of the IM*.

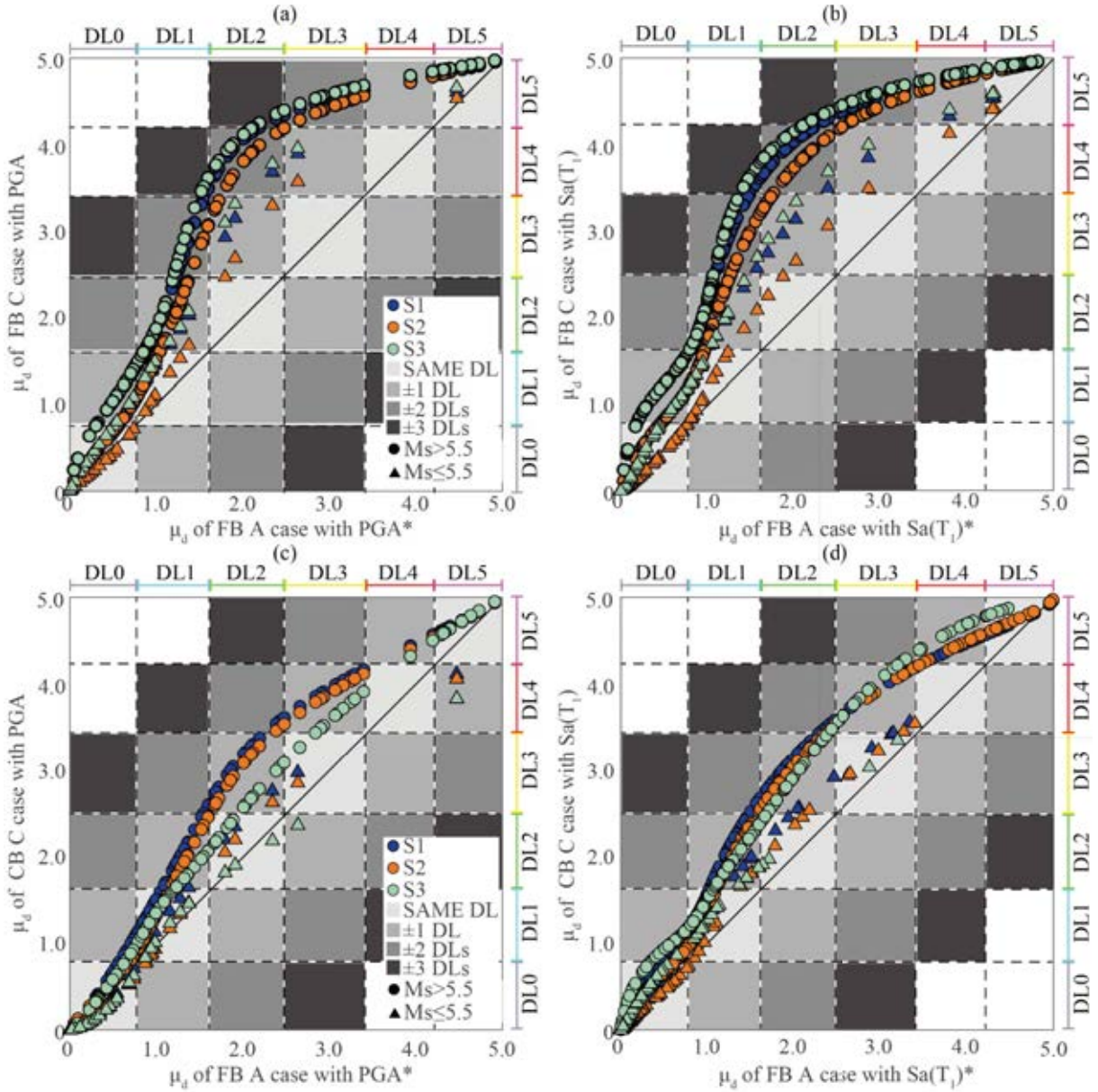

Figure 8: Comparison among the μ_d resulting for the different analyzed cases from the curves expresses as a function of (a) PGA and (b) $Sa(T_1)$ for FB C model, (c) and (d) for CB C model. In the FB A case, the PGA* and $Sa(T_1)$* values - amplified according to the coefficients proposed in the Eurocode 8 ([24]) - were used.

4 CONCLUSIONS

The paper compares the fragility curves and the derived mean damages of a real URM structure ideally placed on stiff rock (FB A) or settled on four different soil profiles. The latter ones include its real foundation subsoil as well as other three with an equivalent shear wave velocity falling in the range of soil type C. The base of the structural model is alternatively assumed as fixed (FB C) or endowed with springs (CB C), simulating in that way the soil-foundation dynamic impedance.

The comparison among the results of the FB A and FB C cases shows the expected increase of the probability of failure when site amplifications are considered.

The comparison among FB C and CB C highlights: i) a general increase in the spectral accelerations affecting the model on springs; ii) a reduction of the probability of failure. As expected, the first effect (i) is due to the period elongation induced by the soil-foundation-structure interaction while the second (ii) is mainly ascribable to the increment of damping associated to the additional energy dissipated by the soil-foundation system.
The comparison among the results of models on the different soil profiles reveals that the highest damage levels are rarely achieved by structures placed on gravel. This is because they are affected by lower seismic actions and benefit of higher soil damping mobilized by the early development of nonlinearity in such soil types. Significant beneficial effects are also recognized for structures settled on soft clay again due to the significant damping mobilized by the considerable strain levels achieved in such profile.
Finally, the mean damages of FB C and CB C were compared with the values resulting from the probability of failures estimated by amplifying the intensity measure through the conventional coefficients proposed by Eurocode [24] to account for the site effects. The comparison shows that such simplified approach underestimates the damage up to two damage levels. Nevertheless, it is currently the most widespread procedure because fragility curves are mostly generated for fixed base structures and without considering site effects through site response analyses. Results achieved could be further developed in future works to improve also practice-oriented procedures.

REFERENCES

[1] A. Sextos, R. De Risi, A. Pagliaroli, S. Pagliaroli, S. Foti, et al., Local site effects and incremental damage of buildings during the 2016 Central Italy Earthquake sequence. *Earthq Spectra*, **34**(4), 1639-1669, 2018.

[2] L. Sorrentino, S. Cattari, F. da Porto, G. Magenes, A. Penna, Seismic behaviour of ordinary masonry buildings during the 2016 central Italy earthquakes. *Bull Earthq Eng*., **17**(10), 5583-5607, 2019.

[3] J.P. Stewart, P. Zimmaro, G. Lanzo, S. Mazzoni, E. Ausilio, et al, Reconnaissance of 2016 central Italy earthquake sequence. *Earthq Spectra*, **34**(4), 1547-1555, 2018.

[4] V. D'Amico, M. Mucciarelli, Validation through HVSR measurements of a method for the quick detection of site amplification effects from intensity data: an application to a seismic area in Northern Italy. *Soil Dyn Earthq Eng*, **22**(6), 475-483, 2002.

[5] N. Chieffo, A. Formisano, Induced seismic-site effects on the vulnerability assessment of a historical centre in the Molise region of Italy: analysis method and real behaviour calibration based on 2002. *Earthq Geosci* **10** (1), 21,2020.

[6] G. Brando, A. Pagliaroli, G. Cocco, F. Di Buccio, Site effects and damage scenarios: The case study of two historic centers following the 2016 Central Italy earthquake. *Engineering Geology*, **272**, 105674, 2020.

[7] A. Pagliaroli, F. Pergalani, A. Ciancimino, A. Chiaradonna, M. Compagnoni, F. de Silva, S. Foti, S. Giallini, G. Lanzo, L. Luzi, L. Macerola, M. Nocentini, A. Pizzi, M. Tallini, C. Teramo, Site response analyses for complex geological and morphological conditions: relevant case-histories from 3rd level seismic microzonation in Central Italy, *Bull. Earthq. Eng.*, Special Issue: "Seismic Microzonation of Central Italy", 2019 https://doi.org/10.1007/s10518-019-00610-7.

[8] G. Lanzo, F. Silvestri, A. Costanzo, A. d'Onofrio, L. Martelli, A. Pagliaroli, S. Sica, A. Simonelli, Site response studies and seismic microzoning in the Middle Aterno valley (L'aquila, Central Italy). *Bull. Earthq. Eng.* **9**, 1417, 2011.

[9] F. Khosravikia, M. Mojtaba M. A. Ghannad, The effect of soil–structure interaction on the seismic risk to buildings. *Bull. Earthq. Eng.,* **16**, 3653-3673, 2018.

[10] S. Casolo, V. Diana, G. Uva, Influence of soil deformability on the seismic response of a masonry tower. *Bull. Earthq. Eng.*, **15**, 1991-2014, 2017.

[11] F. de Silva, Influence of soil-structure interaction on the site-specific seismic demand of masonry towers. *Soil Dyn Earthq Eng*, **131**, 106023, 2020.

[12] A. Bayraktar, E. Hokelekli, Influences of earthquake input models on nonlinear seismic performances of minaret-foundation-soil interaction systems. *Soil Dyn. Earthq. Eng*. **139**, 2020.

[13] A. Karatzetzou, D. Pitilakis, M. Kržan, V. Bosiljkov, Soil-foundation-structure interaction and vulnerability assessment of the Neoclassical School in Rhodes, Greece. *Bull Earthq Eng*, **13**, 411-428, 2015.

[14] A. Fathi, A. Sadeghi, M.R. Emami Azadi, N. Hoveidae, Assessing the soil-structure interaction effects by direct method on the out-of-plane behavior of masonry structures (case study: Arge-Tabriz). *Bull. Earthq. Eng*., 2020 https://doi.org/10.1007/s10518-020-00933-w.

[15] M. Dolce, M. Nicoletti, A. De Sortis, S. Marchesini, D. Spina, F. Talanas, Osservatorio sismico delle strutture: the Italian structural seismic monitoring network. *Bull Earthq Eng* **15**(2), 621-641, 2017.

[16] A. Brunelli, F. de Silva, A. Piro, S. Sica, F. Parisi, F. Silvestri, S. Cattari, Numerical simulation of the seismic response and soil-structure interaction for a monitored masonry school building damaged by the 2016 Central Italy earthquake. *Bull Earthq Eng*., **19**(2), 1181-1211, 2021.

[17] C. Ferrero, P.B. Lourenco, C. Calderini, Nonlinear modeling of unreinforced masonry structures under seismic actions: validation using a building hit by the 2016 Central Italy earthquake. *Frattura ed Integrità Strutturale*, **14**(51), 92-114, 2020.

[18] F. Cavalieri, A.A. Correia, H. Crowley, R. Pinho, Seismic fragility analysis of URM buildings founded on piles: influence of dynamic soil–structure interaction models. *Bull. Earthq. Eng*. **18**, 4127-56, 2020.

[19] D. Peduto, M. Korff, G. Nicodemo, A. Marchese, Empirical fragility curves for settlement-affected buildings: Analysis of different intensity parameters for seven hundred masonry buildings in The Netherlands. *Soils and Foundations*, **59**(2), 380-397, 2019.

[20] F. Jalayer, H. Ebrahimian, A. Miano, G. Manfredi, H. Sezen, Analytical fragility assessment using unscaled ground motion. *Earthquake Engng Struct Dyn.*, 1-25 2017.

[21] C. Smerzini, R. Paolucci, *SIMBAD: a database with Selected Input Motions for displacement Based Assessment and Design* – 3rd release by Department of Structural Engineering, Politecnico di Milano, Italy. Research Project DPC RELUIS, 2013.

[22] I. Iervolino, C. Galasso, R. Paolucci, C. Smerzini, Ground Motion Record Selection Based on Broadband Spectral Compatibility. *Earthq. Spectra*, **30**(4), 1427-1448, 2014.

[23] NTC, *Norme Tecniche per le Costruzioni*. DM 17/1/2018, Italian Ministry of Infrastructure and Transportation, G.U. n. 42, 20 February 2018, Rome, Italy, 2018 (in Italian).

[24] CEN, EN 1998-1, Eurocode 8*: Design of structures for earthquake resistance - Part 1: General rules, seismic actions and rules for buildings*. Brussels: CEN, 2004.

[25] G. Grünthal, *European macroseismic scale EMS-98*. European Seismological Commission, Sub-commission on Engineering Seismology, Working Group Macroseismic Scales, Luxembourg, 1998.

[26] S. Lagomarsino, S. Cattari, PERPETUATE guidelines for seismic performance-based assessment of cultural heritage masonry structures, *Bull Earthq Eng*, **13**(1), 13-47, 2015.

[27] S. Marino, S. Cattari, S. Lagomarsino, Are the nonlinear static procedures feasible for the seismic assessment of irregular existing masonry buildings? *Eng. Struct.*, **200**, 109700, 2019.

[28] MIT, Istruzioni per l'applicazione dell'aggiornamento delle Norme tecniche per le costruzioni di cui al Decreto Ministeriale 17 gennaio 2018, Ministry of Infrastructures and Transportations, Rome, Italy, 2019 (in Italian).

[29] D. Sivori, Ambient vibration tools supporting the model-based seismic assessment of existing buildings. PhD dissertation, University of Genoa, Italy, 2021.

[30] S. Cattari, M. Angiolilli, Procedure for the attribution of EMS98-damage levels in masonry buildings from observed seismic damage or nonlinear analyses, *Bull Earthq Eng*, submitted.

[31] J.J. Bommer, G. Magenes, J Hancock, P. Penazzo, The Influence of Strong-Motion Duration on the Seismic Response of Masonry Structures, *Bull. Earthq. Eng,* **2**, 1-26, 2004.

[32] M. Zucconi, R. Ferlito, L. Sorrentino, Validation and extension of a statistical usability model for unreinforced masonry buildings with different ground motion intensity measures. *Bull. Earthq. Eng*, **18**, 767-795, 2020.

[33] A. Mouyiannou, M. Rota, Selecting appropriate intensity measures for analytical state dependent fragility functions of URM buildings. *16th World Conference on Earthquake*, (16WCEE), Santiago, Chile, January 9-13, 2017.

[34] S. Cattari, D. Camilletti, S. Lagomarsino, S. Bracchi, M. Rota, A. Penna, Masonry Italian Code-Conforming Buildings. Part 2: Nonlinear Modelling and Time-History Analysis. *J. Earthq. Eng.* **22**(2), 2010-2040, 2018.

[35] ReLUIS-Task 4.1 Workgroup report, edited by S. Cattari, S. Degli Abbati, D. Ottonelli, D. Sivori et al. *Report di sintesi sulle attività svolte sugli edifici in muratura monitorati dall'Osservatorio Sismico delle Strutture, Linea Strutture in Muratura*, ReLUIS report, Rete dei Laboratori Universitari di Ingegneria Sismica, 2018 (in Italian).

[36] MZS3, *Report of the 3rd level Seismic Microzonation of Visso village*. Approved by the Working Group, May 29, 2018. https://www.comune.visso.mc.it/avvisi-cms/microzonazione-sismica-iii-livello/.

[37] T. Imai, Y. Yoshimura, Elastic wave velocity and soil properties in soft soil. *Tsuchito-Kiso* **18** (1), 17-22, 1970 (in Japanese).

[38] S.H.H. Lee, Analysis of the multicollinearity of regression equations of shear wave velocities. *Soils and Foundations*, **32**(1), 205-214, 1992.

[39] Y. Ohta, N. Goto, Empirical shear wave velocity equations in terms of characteristic soil indexes. *Earthq. Eng. Struct. Dyn.*, **6**, 167-187, 1978.

[40] A. d'Onofrio, F. Silvestri, Influence of Micro-Structure on Small-Strain Stiffness and Damping of Fine Grained Soil and Effects on Local Site Response. *International Conferences on Recent Advances in Geotechnical Earthquake Engineering and Soil Dynamics*, **15**, 2001.

[41] B. O. Hardin, M. Kalinski, Estimating the Shear Modulus of Gravelly Soils. *J. Geotech. Geoenviron. Eng.*, **131**(7), 2005.

[42] A. Kottke, E.M. R Rathje, *Technical manual for Strata*. Report No. 2008/10. Pacific Earthquake Engineering Research Center, University of California, Berkeley, 2008.

[43] ReLUIS-WorkPakage 1, Deliverable UniNa, *Modellazione delle curve di decadimento del modulo di taglio e del fattore di smorzamento di alcuni terreni dell'Italia Centrale*, ReLUIS report, Rete dei Laboratori Universitari di Ingegneria Sismica (in Italian), 2018.

[44] A. Ciancimino, G. Lanzo, G.A. Alleanza et al, Dynamic characterization of fine-grained soils in central Italy by laboratory testing. *Bull Earthq Eng*, **18**, 5503-5531, 2019.

[45] T. Liao, N. Massoudi, M. Mchood, K.H. Stokoe, M.J. Jung, F.Y. Menq, Normalized shear modulus of compacted gravel. *18th international conference on soil mech Geotech eng.* (ICSMGE), Paris, France, September 2-6, 2013.

[46] W. Ramberg, W.R. Osgood, *Description of stress-strain curves by three parameters*. Natl Advis Comm Aeronaut, Washington DC, 1943.

[47] G. Masing, Eigenspannungen und Verfestigung beim messing. *2nd Int congress of App Mech*, Zurich, Swiss, September 12-17, 1926.

[48] S. Lagomarsino, A. Penna, A. Galasco, S. Cattari, TREMURI program: An equivalent frame model for the nonlinear seismic analysis of masonry buildings. *Eng Struct*, **56**, 1787-1799, 2013.

[49] S. Cattari, G. Magenes, Benchmarking the software packages to model and assess the seismic response of unreinforced masonry existing buildings through nonlinear static analyses. *Bull Earthq Eng*, 2021. https://doi.org/10.1007/s10518-021-01078-0.

[50] G. Gazetas, Formulas and charts for impedances of surface and embedded foundations. *J Geotech Eng*, **117**(9), 1363-1381, 1991.

[51] A. Maravas, G. Mylonakis, D.L. Karabalis, Simplified discrete systems for dynamic analysis of structures on footings and piles. *Soil Dyn Earthq Eng*, **61-62**, 29-39, 2014.

[52] R. Paolucci, A.G. Ozcebe, C. Smerzini, A. Masi, V. Manfredi, Selection and spectral matching of recorded ground motions for earthquake engineering analysis. *Internal report of RELUIS 2019* - WP4, Mappe di rischio e scenari di danno sismico (MARS), 2020.